Facile Fabrication of Hierarchically Structured Silica Coatings from Hierarchically Mesoporous Silica Nanoparticles and Their Excellent Superhydrophilicity and Superhydrophobicity

Xin Du,[†,‡] Xiaoyu Li,[†,‡] and Junhui He*[,†]

Functional Nanomaterials Laboratory and Key Laboratory of Photochemical Conversion and Optoelectronic Materials, Technical Institute of Physics and Chemistry (TIPC), Chinese Academy of Sciences, Zhongguancun Beiyitiao 2, Haidianqu, Beijing 100190, China, and Graduate University of Chinese Academy of Sciences, Beijing 100864, China

ABSTRACT Silica coatings with hierarchical structures were prepared on glass substrates via layer-by-layer assembly using hierarchically mesoporous silica nanoparticles as building block. These coatings demonstrated excellent superhydrophilic properties. After hydrophobic modification, the obtained coatings exhibited hydrophobic properties in the measurements of water contact angles by employing contact-mode and drip-mode, respectively. Water droplet of large volume (15 μL) had a smaller sliding angle than that of small volume (3 μL) when using the contact-mode due to the role of gravity despite the existence of large adhesive force between water droplet and the coating surface, while very small sliding angles were noted when using the drip-mode because of the existence of kinetic energy. The transmittance of fabricated coatings was enhanced and reduced, respectively, in the long and short wavelength ranges as compared with blank slide glass.

KEYWORDS: hierarchical mesostructure • silica nanoparticle • coating • water wettability • layer-by-layer assembly

1. INTRODUCTION

Coatings with extreme wettability such as superhydrophobicity (water contact angle (WCA) larger than 150° and extremely low WCA hysteresis) and superhydrophilicity (WCA less than 5° within 0.5 s or less) have been attracting much attention in material science for their scientific significance, self-cleaning and antifogging properties and numerous potential applications. It is well-known that the wettability of solid surface is controlled by its surface energy, which is determined by its components, and its surface roughness or porosity. Early theoretical works by Wenzel (1), Cassie−Baxter (2), and Quéré (3) and more recent studies (4−33) indicated that the construction of hierarchical micro- and nanostructures with high surface roughness and porosity is an effective approach to tailor the wettability of a surface.

So far, varied components, including silicon (4), silica (13−33), titania (5, 6), zirconia (7), zinc oxide (8), cobalt oxide (9), tin oxide (10), carbon (11), and polymers (12), have been used to prepare coatings and films on glass or silicon substrates with superhydrophobicity, superhydrophilicity, or functionality of mutual conversion between both. Among them, silica as a coating material exhibits promising characteristics such as nontoxicity, high thermal and mechanical stability, easy structural regulation, intrinsically high level of wettability, low dielectric constant, and low refractive index. Methods previously used for constructing hierarchically structured silica coatings on glass or silicon substrates include evaporation induced self-assembly process (13, 14), convective assembly (15), hydrothermal treatment (16), etching (4), spin-coating (17), bar-coating (18, 19), spray-coating (20), direct dip-coating (21, 22), and layer-by-layer (LbL) dip-coating (23−33). In these methods, silica precursors used involve silica sol−gels (13, 14, 21), sodium silicate (26−29), silica hollow spheres (31, 33), mesoporous silica nanoparticles and solid silica nanoparticles with varied sizes and raspberry-like (19, 22, 30) or spherical morphologies (15, 24, 29, 32). Among the various methods, the LbL dip-coating has been proved to be a simple, general, and inexpensive way to fabricate uniform coatings on both flat or nonflat surfaces with large areas.

Very recently, we reported easy fabrication of silica nanospheres with varied morphologies and pore structures, including mesoporous nanospheres, nanospheres with hierarchical pores (from 2 to 100 nm) and hollow nanospheres of mesoporous shell at room temperature simply by regulating the ethanol/ethyl ether volume ratio in the starting

* To whom correspondence should be addressed. Tel.: +86-10-82543535. Fax: +86-10-82543535. E-mail: jhhe@mail.ipc.ac.cn.

Received for review April 29, 2010 and accepted July 2, 2010

† Technical Institute of Physics and Chemistry (TIPC), Chinese Academy of Sciences.

‡ Graduate University of Chinese Academy of Sciences.

DOI: 10.1021/am1003766

solution (34). The novel hierarchically mesoporous silica nanoparticles (HMSNs) may have more advantages than previous particles as building block for constructing surfaces of high roughness because of their unique hierarchical mesoporous structures. Thus we employed HMSNs as building block to fabricate silica coatings on glass substrates via the LbL dip-coating approach. The fabricated coatings presented hierarchical micro- and nanostructures with high surface roughness and porosity, and had unique superhydrophilic properties. After hydrophobic modification, the obtained coatings showed hydrophobic properties in the measurements of WCAs by employing contact-mode and drip-mode, respectively. The sliding angles exhibited large difference between the two different modes of measurement. The fabricated coatings also demonstrated enhanced and reduced transmittances, respectively, in the long and short wavelength ranges as compared with blank slide glass. To the best of our knowledge, such HMSN coatings have not been reported yet.

2. EXPERIMENTAL SECTION

2.1. Materials. Sodium poly(4-styrenesulfonate) (PSS, $M_w \approx$ 70 000) and 1H,1H,2H,2H-perfluorooctyltriethoxysilane (POTS, 97%) were obtained from Alfa Aesar. Poly(diallyldimethylammonium chloride) (PDDA, M_w = 200 000−350 000, 20 wt %) was purchased from Aldrich. Aqueous ammonia (25%), concentrated sulfuric acid (98%), and hydrogen peroxide (30%) were purchased from Beihua Fine Chemicals. Hierarchically mesoporous silica nanoparticles (HMSNs) were prepared according to our previous work (34). In detail, 0.5 g of CTAB was dissolved in an emulsion composed of 70 mL of H_2O, 0.8 mL of aqueous ammonia, 20 mL of ethyl ether, and 10 mL of ethanol. After the mixture was vigorously stirred for 0.5 h at room temperature, 2.5 mL of TEOS was quickly dripped into the mixture. The resulting mixture was vigorously stirred at room temperature for 4 h. A white precipitate was obtained, filtered, washed with pure water, and dried in air at 60 °C for 24 h. CTAB and other organic components in the product were eventually removed by calcination in air at 550 °C for 5 h. HMSNs were used as building block in the preparation of hierarchically structured silica coatings on glass substrates. Pure water with a resistivity higher than 18.2 MΩ cm was used in all experiments, and was obtained by a three-stage Millipore Mill-Q Plus 185 purification system (Academic).

2.2. Preparation of HMSN Coatings with Hierarchical Structure. The procedure for preparation of HMSN coatings with hierarchical structure is divided into three steps and described as follows (30−33). First, commercially available glass or silicon substrates were cleaned with Pirhana solution (98 wt % H_2SO_4/30 wt % H_2O_2, 7/3, v/v) and then washed with pure water (**Caution***: the Pirhana solution is highly dangerous and must be used with great care*). The cleaned substrates were alternately dipped in a PDDA and a PSS solution for 5 min, and redundant polyelectrolytes were removed by shaking in pure water for 2 min and rinsing for 1 min, followed by drying with N_2 flow at room temperature. The concentrations of PDDA and PSS aqueous solutions were 2 mg mL^{-1}. Mutilayers of $(PDDA/PSS)_5$/PDDA were prepared, and were used as a primer in all experiments. Second, the $(PDDA/PSS)_5$/PDDA covered substrates were alternately dipped in a HMSN aqueous suspension (0.5 wt %) and a PDDA solution (2 mg mL^{-1}) by the same procedure for an appropriate number of cycles. Finally, the as-prepared coatings were calcined (heating rate: 1 K min^{-1}) at 550 °C for 3 h to remove the polyelectrolytes.

2.3. Hydrophobic Modification of HMSN Coatings. Hydrophobic modification of HMSN coatings on slide glasses was carried out by a simple chemical vapor deposition (CVD) of POTS (16). The slide glasses with HMSN coatings were placed in a Teflon container, and sealed by stainless steel autoclave, on the bottom of which was dispensed a few droplets (10−20 μL) of POTS. There was no direct contact between the substrate and the POTS droplets. The autoclave was put in an oven at 120 °C for 2 h to enable the vapor of POTS to react with the hydroxyl groups on the coating surface. Finally, the autoclave was opened and placed in an oven at 150 °C for an additional 1.5 h to volatilize unreacted POTS molecules on the coating.

2.4. Characterization. The morphologies of coatings on slide glasses were observed by scanning electron microscopy (SEM) on a Hitachi S-4300 scanning electron microscope operated at 10 kV. Transmission electron microscopy (TEM) observations of HMSNs were carried out on a JEOL JEM-2010 transmission electron microscope operated at an acceleration voltage of 150 kV. Water contact angles (WCAs) of surfaces were measured at ambient temperature on a JC2000C contact angle/interface system (Shanghai Zhongchen Digital Technique Apparatus Co.), the angle precision of which is ±0.5°. Water droplets of an appropriate volume were dropped carefully onto the sample surfaces. Once a water droplet contacted the sample surface, the machine began to take photos at a speed of 30 photos/s, i.e., the interval between the contact moment and the first image was 33 ms. The measurement was carried out on three different areas of the sample surface. Transmittances in the range between 200 and 800 nm were recorded using a TU-1901 spectrophotometer (Beijing Purkinje General Instrument Co.)

3. RESULTS AND DISCUSSION

3.1. Preparation of HMSN Coatings with Hierarchical Structure. As shown in Figure 1a, calcined HMSNs have a size of ca. 150−220 nm, and large mesopores (5−30 nm) can be seen clearly on their surface. The dark and pale parts in the interior of HMSNs (Figure 1b) support the existence of large mesopores on the surface of HMSNs. Small mesopores of 2−3 nm were also observed clearly in the interior of MSNs (inset in Figure 2b). Therefore, HMSNs have a hierarchically mesoporous structure. Nitrogen adsorption−desorption measurements showed that the Brunauer−Emmett−Teller (BET) specific surface area, the pore diameter and pore volume of HMSNs s are 1078 m^2 g^{-1}, 2.7 nm, and 1.01 cm^3 g^{-1}, respectively. Figure 1c exhibits that HMSNs have excellent dispersibility in water, thus making them ideal building block for LbL self-assembly.

Polycation (PDDA) and polyanion (PSS) can be readily adsorbed on the surface of Piranha solution treated slide glasses. As a result, a thin film of desired surface charges can be obtained on the surface of slide glasses. There are many silanol groups on the surface of HMSNs, and the point of zero charge is 2.1 for SiO_2 (the pH value of SiO_2 suspension is ca. 9) (35), which renders the surface of HMSNs slightly negatively charged in aqueous solution. Thus, HMSNs can be adsorbed alternately with PDDA on the surface of slide glass with a primer. To attain desired roughness and voids between HMSNs, we deposited a varied number of PDDA/HMSNs cycles. The attractive long-range van der Waals forces, repulsive electrostatic interaction between the like-charge HMSNs plus the attractive electrostatic interac-

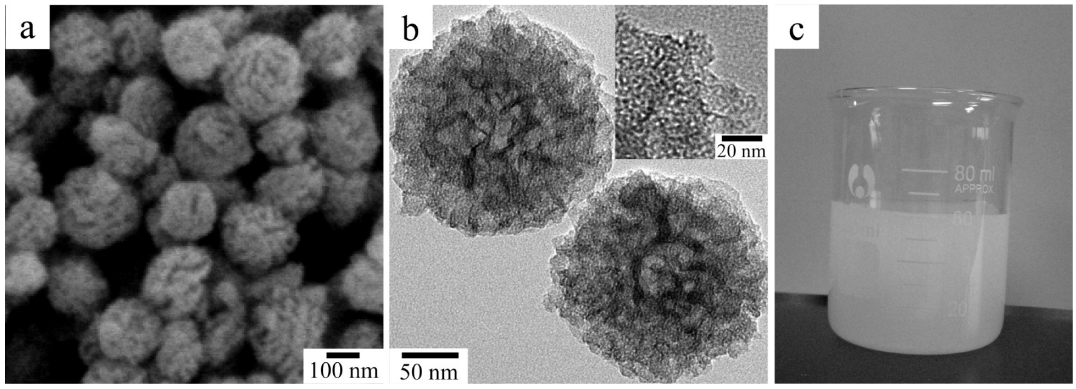

FIGURE 1. (a) SEM and (b) TEM images of calcined HMSNs with hierarchical mesopores. (c) Photograph of aqueous suspension of calcined HMSNs.

tion between HMSNs and the PDDA layer are the critical terms governing the adsorption processes.

SEM images in Figure 2 show the surface morphology of HMSN coatings with PDDA/HMSNs of one through four cycles. Clearly, HMSNs are homogenously scattered on the substrate surface (Figure 2a, c, e, g). Magnified SEM images (Figure 2b, d, f, h) reveal that the coating surface in fact consists of nanometer-sized islands (HMSNs and fragments of HMSNs caused by ultrasonication) and valleys (voids between the islands and large mesopores on the surface of HMSNs). By comparing images b, d, f, and h in Figure 2, it can be seen that the particle density, the coating thickness and surface roughness increase gradually and significantly and the coating presents a three-dimensional network structure more and more clearly with increasing the number of deposition cycles. Obviously, subsequently adsorbed HMSNs would prefer to fill in or sit on the void spaces between HMSNs, thus leading to rougher surfaces and thicker coatings. When four cycles of PDDA/HMSNs were deposited, the coating thickness reached ca. 400 nm, as shown by the cross-sectional image of coating (inset in Figure 2h), and the number and size of voids between HMSNs increased and decreased, respectively, compared with the coatings with fewer deposition cycles (Figure 2h). Compared with solid silica nanoparticles of similar size (32), HMSNs were adsorbed more easily on the surface of slide glasses, as revealed by comparing the particle densities of two coatings obtained under otherwise identical conditions. After calcination and POTS-modification, the morphology and structure of coatings had no significant changes (not shown), indicating the robustness of these HMSN coatings.

3.2. Superhydrophilic Properties of HMSN Coatings. The static WCA was ca. 14° on the surface of slide glass treated by Pirhana solution and stored in pure water for a least one day (Figure S1a). After it was coated with $(PDDA/PSS)_5PDDA$, the static WCA became ca. 37°, indicating less hydrophilicity of polyelectrolytes. Time-dependent changes in WCA on the coating surface before and after calcination are shown in panels a and b in Figure 3, respectively, as a function of the number of deposition cycles of PDDA/HMSNs. The contact mode (Figure 4) was chosen to measure the WCAs, and the volume of water droplets for the measurements was set at 3 μL. Clearly, the WCAs on the coatings decrease quickly with increase of time from 0 to 1000 ms (Figure 3a, b), indicating fast spreading of water droplets. For the coatings before calcination, the initial WCAs and the four WCA-time lines (Figure 3a) do not have a clear trend with increase of the number of deposition cycles, probably because of the presence of polyelectrolytes with less hydrophilicity. The time from initial contact to spreading to 5° is ca. 505, 546, 366, and 367 ms, respectively, for the HMSN coatings of one through four cycles of PDDA/HMSNs. The WCAs (2.9−3.2°) of these coatings after a spreading time of 1000 ms (Figure 3a) are significantly smaller than the static WCA (24°) of the uncalcined coatings of raspberry-like nanoparticles (30). The coatings of three and four deposition cycles of PDDA/HMSNs already had the superhydrophilic property before calcination. After calcination, the time from initial contact to spreading to 5° is ca. 288, 197, 175, and 152 ms, respectively, for the HMSN coatings of one through four cycles of PDDA/HMSNs. Thus, the wettability of the coatings increased significantly compared with that of the uncalcined coatings (Figure 3b), and all these calcined coatings demonstrated superhydrophilicity. The WCAs at identical time in the four WCA-time lines decrease clearly with increase of the number of deposited PDDA/HMSNs cycles. These results indicate that the hydrophilicity of HMSN coating is enhanced with increase of the number of deposition cycles. This may be due to the increases of the number of voids and pores and surface roughness, and all the increases would lead to a larger contact area between water droplet and coating, thus improving the hydrophilicity according to the Wenzel model (1). These results agree with the SEM observations shown in Figure 2. The time from initial contact to spreading flat (WCA: 0°) is 600 ms (Figure 3b) on the calcined HMSN coating of four deposition cycles, significantly shorter than that (ca. 840 ms) of a multilayer coating assembled sequentially with two deposition cycles of 150 nm solid silica nanoparticles and two deposition cycles of 30 nm solid silica nanoparticles (32). This indicates that the hierarchically mesoporous silica nanoparticles HMSNs offered additional enhancement of hydrophilicity compared with solid silica nanoparticles. The hierarchical micro- and nanostructures of the HMSN coatings, which were constructed by MSNs with hierarchical mesopores, must

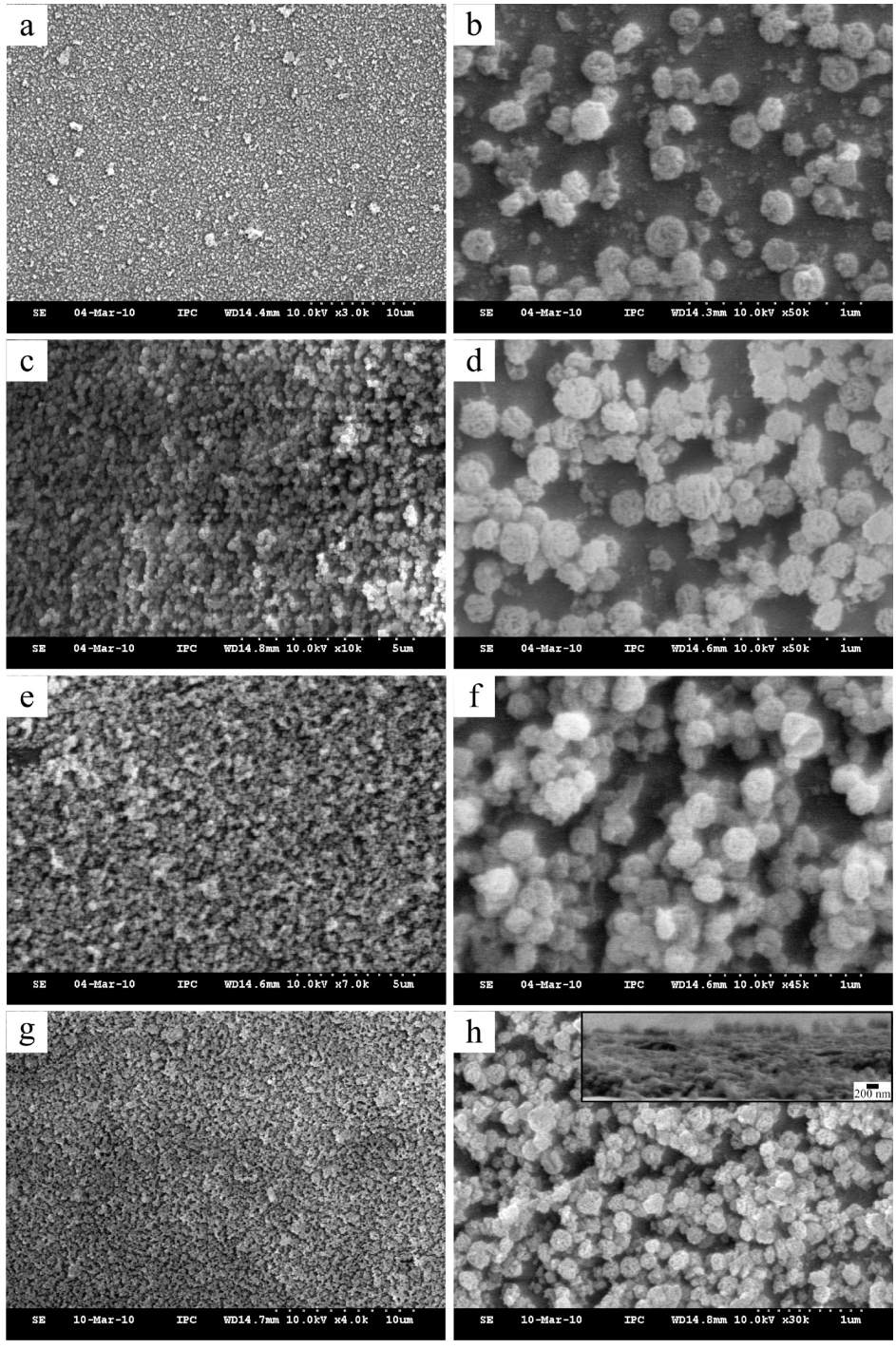

FIGURE 2. SEM images of HMSN coatings on slide glasses by alternate LbL deposition of PDDA/MSNs of: (a, b) one cycle, (c, d) two cycles, (e, f) three cycles, and (g, h) four cycles. The inset in (h) is the cross-sectional SEM image of the coating.

have enhanced the hydrophilicity by even faster absorption and spreading of water droplets (25, 30−33).

3.3. Hydrophobic Properties of POTS-Modified HMSN Coatings. The contact-mode (Figure S2a−d in the Supporting Information and Figure 4a−d) and drip-mode (Figure 4e−g) were chosen to measure the WCAs on the coatings after hydrophobic modification, respectively, and the volumes of water droplets for the measurements were 3 μL and slightly smaller than 15 μL for the contact-mode, and 15 μL for the drip-mode, respectively. In fact, water droplets with a volume of ca. 1−14 μL could not be dropped freely using microsyringe because of the large capillary force between water droplet and the tube of microsyringe (Figure 4a and Figure S2a in the Supporting Information), whereas 15 μL is the sole standard volume supplied by the peristaltic pump of our contact angle/interface system. We chose at least three different locations on the coatings, and there were very little difference in the WCAs measured at these locations, indicating the uniformity of the coating surfaces.

When water droplets of 3 μL were used in the contact-mode (Figure S2a−d in the Supporting Information), static WCA on the surface of POTS-modified coating increased

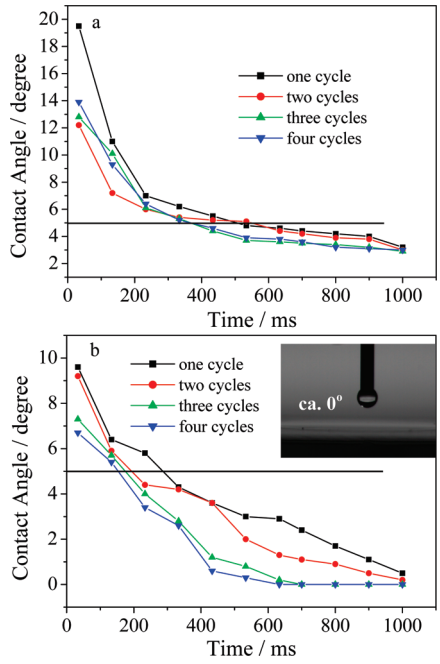

FIGURE 3. Time-dependent changes in WCA on HMSN coatings (a) before and (b) after calcination as a function of the number of deposition cycles of PDDA/HMSNs. The inset in (b) is the digital image of ca. 0° WCA on a porous HMSN coating.

from 136.4 to 151.1° with increase of the number of deposition cycles of PDDA/HMSNs (Figure 5a–d). However, the water droplets did not slide even when the substrates were tilted vertically or turned upside down by hand manipulation, indicating the water droplets adhered tightly to the coating surfaces. This might be because of the existence of large adhesive force between the coating and water droplet using the contact-mode. In the measurement, a water droplet of 3 μL was extruded from the tube of microsyinge toward the coating surface. The substrate with the coating was raised to touch and press the droplet in order to increase the adhesive force between the coating and the water droplet so that the water droplet adhered on the coating surface (Figure 4b). Many times of this trial were needed to make water droplet adhere onto the coating surface because of high hydrophobicity. Water droplet did not adhere to the coating surface until the adhesive force between the coating and water droplet was larger than the capillary force between water droplet and the tube of microsyinge (Figure 4c). In fact, the larger the pressing force, the smaller the WCA (36, 37). Considering the large adhesive force between water droplet and the rough coating surface, which was caused by pressing the water droplet with the coating surface, water droplet may have penetrated into the voids and pores of coating. This probably led to a large sliding angle because the water droplet had to overcome a large resistance (friction) to slide.

When water droplets of slightly smaller than 15 μL were used in the contact-mode, the water droplets easily adhered on the coating surface under slight pressure due to the role of gravity. And the static WCA increases from 128.3° to 145.6° with increase of the number of deposition cycles of PDDA/HMSNs (Table 1 and Figure 5e–h). Compared with water droplets of 3 μL, all the WCAs measured using water droplets of 15 μL on the coatings with identical deposition cycles decrease because of the role of gravity. Similar observations were also reported previously, which showed that the larger the volume of water droplet, the smaller the WCA (38). The sliding angles on the surface of slide glass coated with one, two, three, and four cycles of PDDA/HMSNs were >30, > 30 (see Figure S3 in the Supporting Information), 11.5 ± 1, and 4.5 ± 1° (Figure S4 in the Supporting Information), respectively (Table 1) (30° is the maximum tilt angle of the apparatus). In the contact mode, the significant difference in the sliding angles using water droplets of 3 and 15 μL may mainly result from the difference in gravity and adhesive force due to different volumes. Water droplets of larger volumes may have a smaller sliding angle because of larger gravity despite having a larger adhesive force as well.

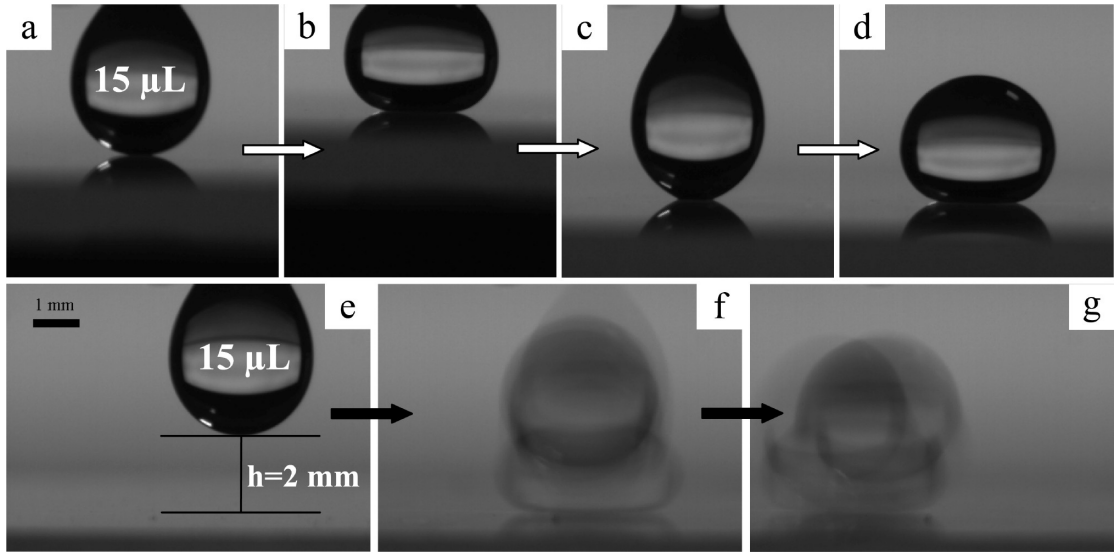

FIGURE 4. Digital images of typical dynamic shapes of water droplets using the contact-mode (a–d, 15 μL) and drip-mode (e–g, 15 μL), respectively. The slide glass was coated with three cycles of PDDA/HMSNs followed by calcination and POTS modification.

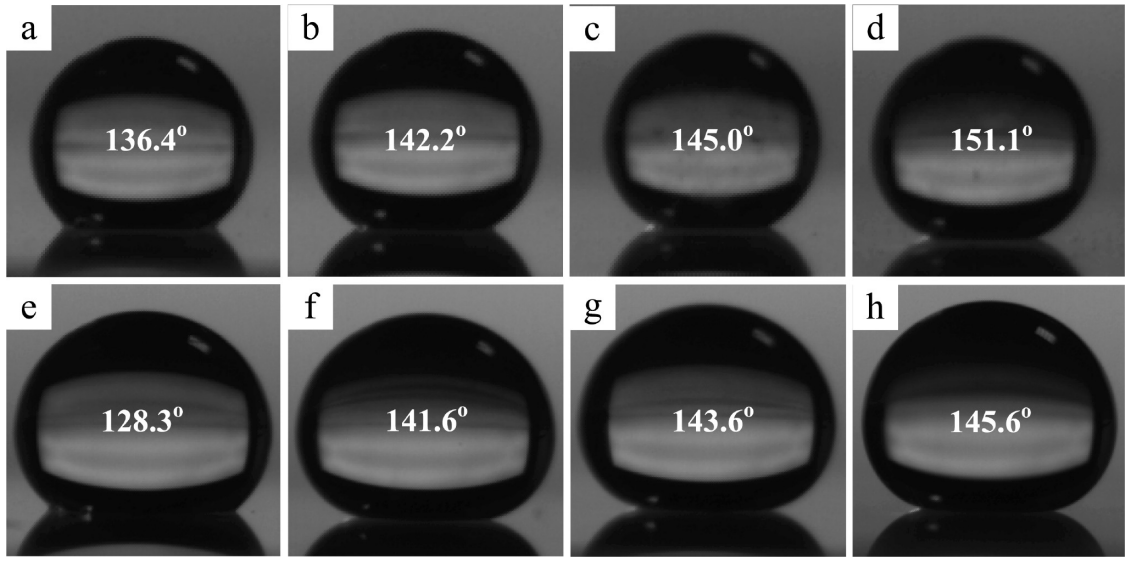

FIGURE 5. Digital images of WCAs on the surface of POTS-modified HMSN coatings with varied numbers of deposition cycles of PDDA/HMSNs: (a, e) one cycle, (b, f) two cycles, (c, g) three cycles, and (d, h) four cycles. The volumes of water droplets in (a−d) and (e−h) were 3 and 15 μL, respectively.

Table 1. WCAs on the Surfaces of Coatings after Hydrophobic Modification

no. of HMSNs cycles	static angle (deg)	advancing angle (deg)	receding angle (deg)	hysteresis of contact angle (deg)	sliding angle (deg) for 15 μL water droplet
1	128.3 ± 1				>30
2	141.6 ± 1				>30
3	143.6 ± 1	149 ± 1	130 ± 1	19 ± 2	11.5 ± 1
4	145.6 ± 1	154 ± 1	144 ± 1	10 ± 2	4.5 ± 1

In the drip mode, if dripped water droplets stopped on the surface and kept steady, the static WCAs were nearly the same as those in the contact mode on the coatings with identical deposition cycles. It was observed that water droplets could roll off the coatings easily and quickly (Figure 4f, g) except for the coating with one deposition cycle of PDDA/HMSNs. The water droplet could not roll off the coating with one deposition cycle of PDDA/HMSNs even when the tilt angle was above 30°. Thus, water droplets can roll off the coating surfaces with a WCA larger than 141° (measured using water droplets of 15 μL).

In the drip mode, the water droplet of 15 μL could roll off the coatings easily and quickly and the possible reason may result from the kinetic energy of water droplet. When a water droplet drops from the tube of microsyinge down to the coating, it would have a momentum of 5.94×10^{-10} kg m s^{-1} and a kinetic energy of 5.88×10^{-11} J, which were estimated roughly from Figure 4e on the assumption of spheroid water droplet. Thus, the water droplet with the momentum and kinetic energy was able to overcome the adhesive force between the coating and the droplet of water, and rolled off the coating easily and quickly. During the sliding process, the water droplet may have not penetrated into the voids and pores of coating. Thus, the water droplet could roll off the coating easily and quickly.

In fact, when water streams from the washing bottle or water pipe flowed onto the surface of the coating, it was very difficult for it to stand on the surface and simply rolled away quickly. Therefore, superhydrophobicity with extremely large WCAs (≥150°) may not be necessary toward a goal of self-cleaning by rain, and the current coating may have already met the requirements. Figure 6 exhibits a photograph of two water droplets of 15 μL on the POTS-modified HMSN coating with four deposition cycles of PDDA/HMSNs. This photograph shows that the coating has good hydrophobicity and is uniform. Identical WCAs were observed after storing the coatings in a Petri dish for more than 1 week, indicating a high stability of hydrophobicity.

3.4. Transmission Spectra of HMSN coatings.

Figure 7 shows the transmission spectra of blank slide glass and slide glasses coated with PDDA/HMSNs of one through four cycles under three situations of as-prepared coatings (Figure 7a), calcined coatings (Figure 7b) and POTS-modified coatings (Figure 7c). It is noted that the transmittance of slide

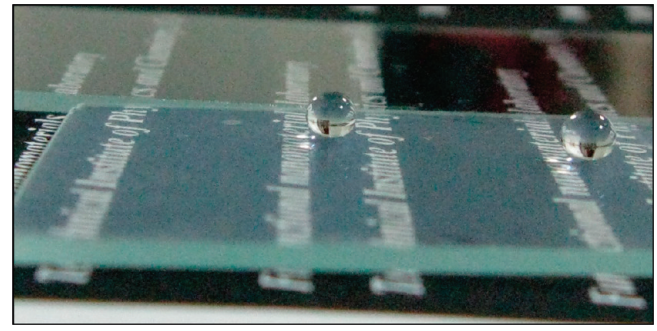

FIGURE 6. Digital image of two water droplets with a volume of 15 μL on POTS-modified HMSN coating obtained by depositing four cycles of PDDA/HMSNs followed by calcination and POTS modification.

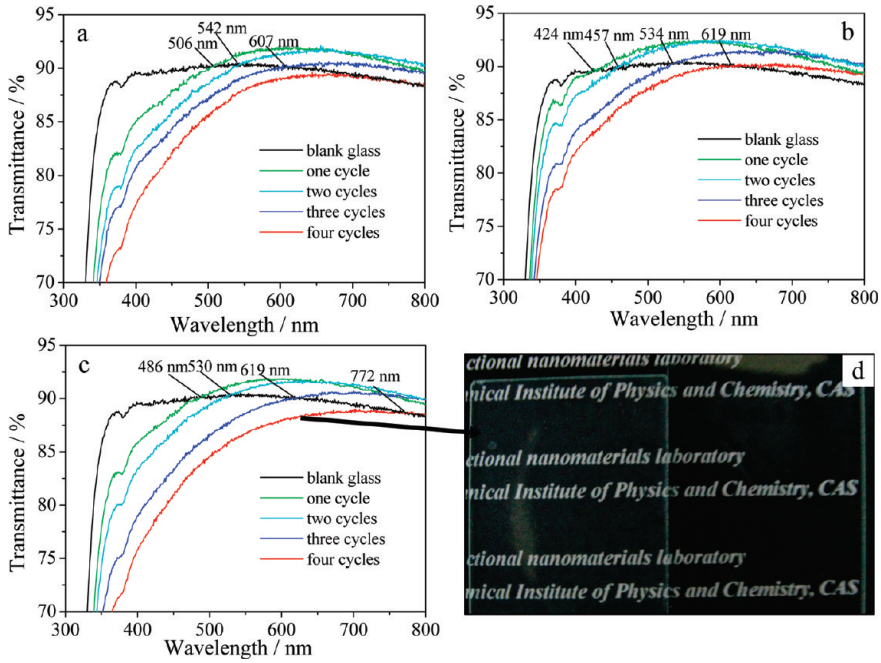

FIGURE 7. Transmission spectra of blank slide glass and slide glasses coated with PDDA/HMSNs of one through four cycles: (a) as-prepared coatings, (b) calcined coatings, and (c) POTS-modified coatings. (d) Digital image taken under lamp light comparing blank slide glass (right) with slide glass coated with four cycles of PDDA/HMSNs after POTS-modification (left).

glass with coating decreases with an increase of the number of deposition cycles of PDDA/HMSNs in the UV−visible range. It is also noted, however, that this trend does not apply completely in the near-infrared range. Especially, the slide glasses with two and three deposition cycles after calcination exhibited higher transmittances in the near-infrared range than that with one deposition cycle. Okubo and co-workers reported that an appropriate thickness for antireflective coatings is estimated to be 95−125 nm (18). For the as-prepared coatings, the transmittance was enhanced and reduced, respectively, in the long and short wavelength ranges as compared with blank slide glass. And the maximum transmittance reached 92.0% by one deposition cycle of PDDA/HMSNs. The increased transmittance is attributed to the high porosity of the coating (18, 24, 32) because of the use and assembly of HMSNs, which will significantly reduce the refractive index of the coating. After calcination, the transmittance of coating was enhanced compared with that of the as-prepared coating, which is probably attributed again to the enhancement of the coating porosity but in this case by removal of polyelectrolytes. The maximum transmittance wavelengths were estimated to be ca. 570, 594, 651, and 675 nm, respectively, for the slide glasses with HMSN coatings by calcining PDDA/HMSNs of one through four cycles, thus exhibiting a red-shift trend. These results indicate that the thicker the coating is, the longer the maximum transmittance wavelength is, agreeing well with the formula: $\lambda = 4nd$, where d is the film thickness, λ is the wavelength of light, and n is the refractive index of coating. After POTS-modification, the transmittance of coating had a little reduction as compared with that of the calcined coating. A comparison photograph of blank slide glass (right) and slide glass coated by four cycles of PDDA/NPs after POTS-modification (left, with the lowest transmittance in Figure 7c) shows that the words can be seen clearly although the coating looks a bit white (Figures 7d and 6).

4. CONCLUSION

In summary, silica coatings with hierarchical structure were facilely prepared on glass substrates via layer-by-layer assembly using hierarchically mesoporous silica nanoparticles as building block, which provide the coatings with abundant nanovoids and nanoreservoirs, and thus extremely large surface area. These coatings demonstrated excellent superhydrophilic properties. After hydrophobic modification, the obtained coatings exhibited hydrophobic properties in the measurements of water contact angles by employing the contact mode and drip mode, respectively. Water droplet of large volume (15 μL) had a smaller sliding angle than that of small volume (3 μL) when using the contact mode because of the role of gravity despite the existence of large adhesive force between water droplet and the coating surface, whereas very small sliding angles were noted when using the drip mode because of the existence of momentum and kinetic energy of water droplets. The comparison of the two modes enhanced the understanding of hydrophobic results. The transmittance of the current coatings was enhanced and reduced, respectively, in the long and short wavelength ranges as compared with blank glass slide. The current coatings may have potential applications as transparent self-cleaning coatings, catalyst supports, chemical sensors, and electronic and electrochemical devices.

Acknowledgment. This work was supported by the Knowledge Innovation Program of the Chinese Academy of Sciences (CAS) (Grant KGCX2-YW-370, KGCX2-YW-111-5), the National Natural Science Foundation of China-NSAF (Grant 10776034), the National Natural Science Foundation of China (Grant 20871118), "Hundred Talents Program" of

CAS, and "Graduate Science and Social Practice Special Funding Innovative Research Program" of CAS.

Supporting Information Available: Additional digital images of water contact angles and sliding angles (PDF). This material is available free of charge via the Internet at http://pubs.acs.org.

REFERENCES AND NOTES

(1) Wenzel, R. N. *Ind. Eng. Chem.* **1936**, *28*, 988–994.
(2) Cassie, A. B. D.; Baxter, S. *Trans. Faraday Soc.* **1944**, *40*, 546–551.
(3) Bico, J.; Thiele, U.; Quéré, D. *Colloid Surf., A* **2002**, *206*, 41–46.
(4) Qi, D.; Lu, N.; Xu, H.; Yang, B.; Huang, C.; Xu, M.; Gao, L.; Wang, Z.; Chi, L. *Langmuir* **2009**, *25*, 7769–7772.
(5) Takeuchi, M.; Sakamoto, K.; Martra, G.; Coluccia, S.; Anpo, M. *J. Phys. Chem. B* **2005**, *109*, 15422–15428.
(6) Tang, H.; Wang, H.; He, J. *J. Phys. Chem. C* **2009**, *113*, 14220–14224.
(7) Han, J. T.; Zheng, Y.; Cho, J. H.; Xu, X.; Cho, K. *J. Phys. Chem. B* **2005**, *109*, 20773–20778.
(8) Badre, C.; Pauporté, T. *Adv. Mater.* **2009**, *21*, 697–701.
(9) Li, L.; Li, Y.; Gao, S.; Koshizaki, N. *J. Mater. Chem.* **2009**, *19*, 8366–8371.
(10) Zhu, W.; Feng, X.; Feng, L.; Jiang, L. *Chem. Commun.* **2006**, 2753–2755.
(11) Feng, L.; Yang, Z.; Zhai, J.; Song, Y.; Liu, B.; Ma, Y.; Yang, Z.; Jiang, L.; Zhu, D. *Angew. Chem., Int. Ed.* **2003**, *42*, 4217–4220.
(12) Zhu, Y.; Hu, D.; Wan, M.; Jiang, L.; Wei, Y. *Adv. Mater.* **2007**, *19*, 2092–2096.
(13) Lu, Y.; Fan, H.; Doke, N.; Loy, D. A.; Assink, R. A.; Lavan, D. A.; Brinker, C. J. *J. Am. Chem. Soc.* **2000**, *122*, 5258–5261.
(14) Fan, H.; Reed, S.; Baer, T.; Schunk, R.; López, G. P.; Brinker, C. J. *Microporous Mesoporous Mater.* **2001**, *44*–*45*, 625–637.
(15) Prevo, B. G.; Hwang, Y.; Velev, O. D. *Chem. Mater.* **2005**, *17*, 3642–3651.
(16) Liu, X.; He, J. *Langmuir* **2009**, *25*, 11822–11826.
(17) Su, C.; Li, J.; Geng, H.; Wang, Q.; Chen, Q. *Appl. Surf. Sci.* **2006**, *253*, 26332636..
(18) Hoshikawa, Y.; Yabe, H.; Nomura, A.; Yamaki, T.; Shimojima, T.; Okubo, T. *Chem. Mater.* **2010**, *22*, 12–14.
(19) Ming, W.; Wu, R.; van Benthem, R.; de With, G. *Nano Lett.* **2005**, *5*, 2298–2301.
(20) Manoudis, P. N.; Karapanagiotis, I.; Tsakalof, A.; Zuburtikudis, I.; Panayiotou, C. *Langmuir* **2008**, *24*, 11225–11232.
(21) Zhao, D.; Yang, P.; Melosh, N.; Feng, J.; Chmelka, B. F.; Stucky, G. D. *Adv. Mater.* **1998**, *10*, 1380–1385.
(22) Qian, Z.; Zhang, Z.; Song, L.; Liu, H. *J. Mater. Chem.* **2009**, *19*, 1297–1304.
(23) Lvov, Y.; Ariga, K.; Onda, M.; Ichinose, I.; Kunitake, T. *Langmuir* **1997**, *13*, 6195–6203.
(24) Rouse, J. H.; Ferguson, G. S. *J. Am. Chem. Soc.* **2003**, *125*, 15529–15536.
(25) Cebeci, F.Ç.; Wu, Z.; Zhai, L.; Cohen, R. E.; Rubner, M. F. *Langmuir* **2006**, *22*, 2856.
(26) He, J.; Fujikawa, S.; Kunitake, T.; Nakao, A. *Chem. Mater.* **2003**, *15*, 3308–3313.
(27) Zhang, L.; Chen, H.; Sun, J.; Shen, J. *Chem. Mater.* **2007**, *19*, 948–953.
(28) Zhang, L.; Li, Y.; Sun, J.; Shen, J. *Langmuir* **2008**, *24*, 10851–10857.
(29) Li, Y.; Liu, F.; Sun, J. *Chem. Commun.* **2009**, 2730–2732.
(30) Liu, X.; He, J. *J. Colloid Interface Sci.* **2007**, *314*, 341–345.
(31) Liu, X.; Du, X.; He, J. *ChemPhysChem* **2008**, *9*, 305–309.
(32) Liu, X.; He, J. *J. Phys. Chem. C* **2009**, *113*, 148–152.
(33) Du, X.; Liu, X.; Chen, H.; He, J. *J. Phys. Chem. C* **2009**, *113*, 9063–9070.
(34) Du, X.; He, J. *Langmuir* **2010**, *26*, 10057–10062.
(35) Zhang, X. T.; Sato, O.; Taguchi, M.; Einaga, Y.; Murakami, T.; Fujishima, A. *Chem. Mater.* **2005**, *17*, 696–700.
(36) Lafuma, A.; Quéré, D. *Nat. Mater.* **2003**, *2*, 457–460.
(37) Bico, J.; Marzolin, C.; Quéré, D. *Europhys. Lett.* **1999**, *47*, 220–226.
(38) Yoshimitsu, Z.; Nakajima, A.; Watanabe, T.; Hashimoto, K. *Langmuir* **2002**, *18*, 5818–5822.

AM1003766